analytical chemistry

pubs.acs.org/ac Article

Sensitive, Highly Stable, and Anti-Fouling Electrode with Hexanethiol and Poly-A Modification for Exosomal microRNA Detection

Guanyu Chen,[⊥] Wenqian Chen,[⊥] Lilan Xu, Huixuan Jin, Weiming Sun, Jianming Lan, Fang Wu, Xi Zhang,* Jing Zhang,* and Jinghua Chen*

Cite This: *Anal. Chem.* 2022, 94, 5382−5391 Read Online

ACCESS | Metrics & More | Article Recommendations | Supporting Information

ABSTRACT: It remains a huge challenge to integrate the sensitivity, stability, reproducibility, and anti-fouling ability of electrochemical biosensors for practical applications. Herein, we propose a self-assembled electrode combining hexanethiol (HT), poly-adenine (poly-A), and cholesteryl-modified DNA to meet this challenge. HT can tightly pack at the electrode interface to form a hydrophobic self-assembled monolayer (SAM), effectively improving the stability and signal-to-noise ratio (SNR) of electrochemical detection. Cholesteryl-modified DNA was immobilized at the electrode through the hydrophobic interaction with HT to avoid the competition between the SAM and the DNA probe on the gold site. Thus, the assembly efficiency and uniformity of the DNA probe as well as the detection reproducibility were increased remarkedly. Poly-A was added on the HT assembled electrode to occupy the unreacted sites of gold to further enhance the anti-fouling ability. The combination of HT and poly-A allows the electrode to ensure favorable anti-fouling ability without sacrificing the detection performance. On this basis, we proposed a dual-signal amplification electrochemical biosensor for the detection of exosomal microRNAs, which showed excellent sensitivity with a detection limit down to 1.46 aM. Importantly, this method has been successfully applied to detect exosomal microRNA-21 in cells and human serum samples, proving its potential utility in cancer diagnosis.

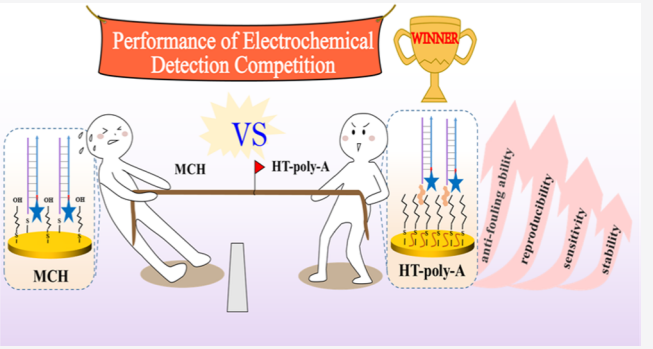

INTRODUCTION

DNA electrochemical biosensors have begun to exhibit great value in disease diagnosis due to their inherent advantages such as high sensitivity, rapid analysis, easy miniaturization, and low cost.[1,2] However, the adoption of electrochemical biosensors in clinical settings is still challenging due to their other characteristics, such as poor stability and reproducibility, proneness to biofouling, and more. To translate proof-of-principle studies into clinical sample detection with cancer patients, there is an urgent need to overcome the issues mentioned above to meet the requirements in clinical settings.

To improve the detection performance, early works mostly focused on constructing a 6-mercaptohexanol (MCH) self-assembled monolayer (SAM) on the electrode interface. However, the progressive degradation of the bioelectronic interface during continuous electrochemical interrogation[3] or the shedding of the sulfydryl-labeled DNA probe caused by competition with MCH limited its application.[4] Better impressive anti-fouling performance has been achieved by more recent proposals, which were focused on developing an innovative anti-fouling surface, such as polymer brushes,[5] SAMs of zwitterionic structures,[6] cross-linked bovine serum albumin (BSA) nanocomposite coating,[7] anti-fouling peptides,[8] and so on. Yet, other critical issues influenced their biosensing application, such as low sensitivity caused by the obstruction of electron transport,[9] poor stability due to the desorption under widespread reducing conditions,[10] and high cost of preparation due to the introduction of expensive nanoparticles. Currently, the development of a simple and low-cost assembly layer that can integrate outstanding detection performance with excellent anti-fouling ability is still a challenge.

For this reason, we designed a hexanethiol (HT)−poly-adenine (poly-A) self-assembled layer. In this design, HT was selected to replace MCH because the structure of the hydrophobic alkyl chains made them tightly packed at the

Received: January 6, 2022
Accepted: March 15, 2022
Published: March 24, 2022

https://doi.org/10.1021/acs.analchem.2c00069
Anal. Chem. 2022, 94, 5382−5391

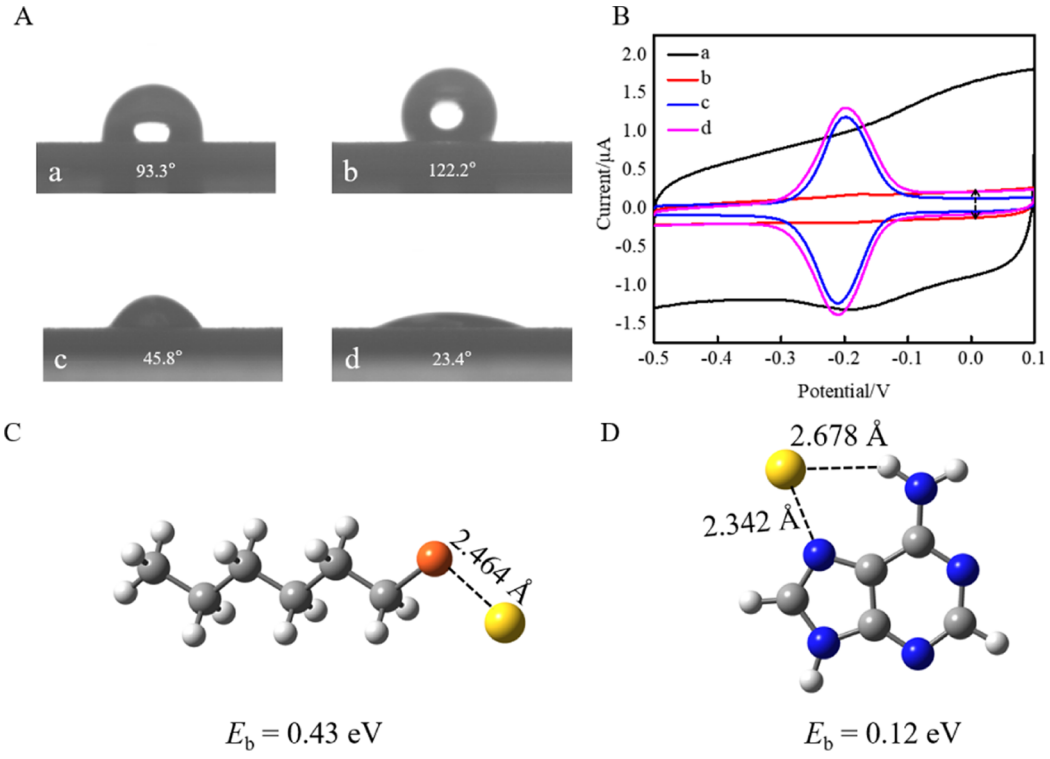

Figure 1. Characterization of electrode interface by (A) water contact angle and (B) CV: (a) GE, (b) GE/HT, (c) GE/HT/Cp, and (d) GE/HT/Cp/poly-A. The structural sketch map of Au atom binding to (C) HT and (D) poly-A. Gray, white, orange, blue, and yellow balls represent carbon, hydrogen, sulfur, nitrogen, and gold atoms, respectively. The interaction between Au and its binding site is indicated by dotted lines.

electrode interface, thereby enhancing the stability[3] and achieving a higher signal-to-noise ratio (SNR). The DNA immobilization through HT also further improved the reproducibility of the detection and the efficiency of assembly. To improve the anti-fouling ability, a layer of poly-A was coated on the HT assembled electrode, which has an affinity for gold, thus effectively decreasing the non-specific adsorption by binding to unreacted gold electrode (GE) sites.[11]

To confirm the performance of the HT−poly-A self-assembled layer-based biosensor in clinical settings, exosomal microRNAs (miRNAs) were chosen as the detection target, and an enzyme-assisted dual signal amplification strategy was proposed to enhance the sensing sensitivity.[12,13] Benefiting from the HT−poly-A self-assembled layer and amplification reactions, the proposed biosensor provided outstanding amplification efficiency and sensitivity of the electrochemical assay with a detection limit down to 1.46 aM. This method can also be applied in complex biological fluids, such as the analysis of serum samples in our case.

EXPERIMENTAL SECTION

Materials. All the DNA oligonucleotides and miRNAs were purchased from Shanghai Sangon Biotech and TaKaRa Biotechnology Co., Ltd. All of them were purified by high-performance liquid chromatography (HPLC). The relevant sequence information is listed in Table S1. The HT was obtained from Shanghai Macklin Biochemical Co., Ltd. MCH, trichloroethyl phosphate (TCEP), and streptavidin modified magnetic beads (SAmbs) were obtained from Sigma-Aldrich Company. MiScript II RT kit and miScript SYBR Green PCR kit were obtained from German Qiagen Corporation. The Nt.BbvCI and Bst DNA polymerase enzymes were obtained from New England Biotechnology Co., Ltd. Deoxyadenosine triphosphate (dATP), deoxythymidine triphosphate (dTTP), deoxycytidine triphosphate (dCTP), and methylene blue (MB) were obtained from Shanghai Aladdin Biochemical Technology Co., Ltd. All aqueous solutions were prepared by Milli-Q water (18.2 MΩ/cm), and all chemicals in the experiment were of analytical grade.

Electrode Treatment and Construction of the HT-Ploy-A Assembled Electrode Interface. The surface of the GE was polished with 0.3 and 0.05 μm alumina and ultrasonically cleaned with deionized water and anhydrous ethanol for 1 min, respectively. After nitrogen drying, the GE was immersed in 0.5 M H_2SO_4 and cyclic voltammetry (CV) curves were scanned by an electrochemical analyzer (CHI 1040C, Shanghai Chenhua Instrument Co., Ltd) until the curves were stable.[14] The scanning potential of CV ranged from −0.35 to +1.5 V, and the standing time, scanning rate, and sampling interval were 2 s, 0.1 V/s, and 1 mV, respectively. The polished electrode was immersed in 100 μL of 5 mM HT solution and reacted at room temperature for 1 h. Then, 4 μL of 1 μM cholesteryl-modified capturing probe (Cp) was dropped on the electrode surface and the electrode was kept at room temperature for 1 h. Then, the assembled electrode was immersed in 100 μL of 1 μM poly-A for 30 min at room temperature to construct the anti-fouling electrode interface.

Preparation of Fuel-Driven Strand Displacement Reaction. Fuel-driven strand displacement reaction (FDSDR) was prepared according to the methods provided in the literature.[15] All DNAs were dissolved in 1× TE buffer (contain 10 mM Tris−HCl pH 7.4, 1 mM EDTA) at a concentration of 100 μM and were diluted in 1× TAE buffer [containing 12.5 mM $(CH_3COO)_2Mg$, 10 mM Tris, and 1.0 mM EDTA·2Na] for subsequent experiments. For FDSDR, 5 μL of 16 μM F and 5 μL of 16 μM S were mixed at 95 °C for 5

https://doi.org/10.1021/acs.analchem.2c00069
Anal. Chem. 2022, 94, 5382−5391

min. Then, the solution was cooled to 25 °C for 30 min to form F−S dsDNA and stored at 4 °C. Then, 10 μL of 20 μM F, 8 μL of 10 U/μL Nt.BbvCI, and 10 μL of different concentrations of miRNA-21 (miR-21) were mixed in 52 μL 1× CutSmart buffer at 37 °C and incubated for 8 h. F2 was still in the supernatant after separating the unwanted strands by magnetic beads. The supernatant (4 μL) was then dropped onto the HT−poly-A coating electrode interface, and the electrode was incubated at room temperature for 1 h.

Preparation of Primer Exchange DNA Amplification Reaction and Electrochemical Biosensor. The above assembled electrode was immersed in a primer exchange DNA amplification reaction (PEDAR) solution and incubated at 37 °C for 2 h to form long strands of DNA on the electrode surface. The PEDAR solution was prepared according to the literature.[1,16] In brief, 5 μL of 10× PBS, 5 μL of 10 mM dATP/dTTP/dCTP, 5 μL of 100 mM $MgCl_2$, 5 μL of 100 μM Tp, 5 μL of 10 μM Tp-clean, and 7.5 μL of 8000 U/mL Bst DNA polymerase were mixed in 17.5 μL DEPC water thoroughly and incubated at 37 °C for 15 min before use. Finally, the electrode was immersed in 100 μM MB for 5 min, and the remaining MB was washed by pure water. The MB adsorbed on the DNA was used as an indicator of electrochemical signal.

RESULTS AND DISCUSSION

Principle of the HT−Poly-A Assembled Electrode. As illustrated in Figure S1, HT is first assembled on the surface of the GE by binding of Au−S to form a hydrophobic alkyl chain layer. Cholesteryl-modified Cp is immobilized at the electrode interface by a hydrophobic interaction between the cholesterol-alkyl chains. Also, through the affinity between gold and adenine, poly-A is deposited at the gold interface to further improve the anti-fouling ability of the electrode.

Characterization of Assembly of the Electrode Interface. Considering that SAM can act as a molecular blocking layer to restrain undesired gold-electrocatalyzed reactions, such as the reduction of molecular oxygen, by occupying existing active sites on the gold surface,[3] the assembly of HT was verified by testing the inhibition of the oxygen reduction reaction at the electrode interface. As shown in Figure S2, no significant reduction peak was observed for either HT (curve a) or MCH (curve b) as compared to that of the bare GE (curve c). This was mainly attributed to the successful assembly of HT and MCH, where the reduction reaction of gold surface oxygen was inhibited. Notably, the HT assembled electrode showed a smaller reduction current than that of MCH, suggesting that HT formed a tighter monolayer than MCH did at the electrode interface.[3] To further confirm this, the covering densities of HT and MCH SAM on the electrode surface were calculated by reductive desorption of CV in degassed 100 mM KOH solution.[17] As shown in Figure S3, the obtained surface coverage density of HT and MCH was 9.85×10^{-9} and 5.76×10^{-9} mol/cm^2, respectively, indicating that HT has a higher surface coverage density.

Water contact angles of electrodes during different assembly processes were measured. After assembly of hydrophobic HT, the hydrophobicity of the electrode surface was significantly improved compared to that of the GE as the water contact angle increased from 93.3 to 122.2° (Figure 1Aa,b), indicating the decrease in wettability of the electrode interface and thereby the tight packing of HT SAM.[18] Subsequently, the assembly of Cp (Figure 1Ac) and poly-A (Figure 1Ad) reduced the water contact angle on the electrode surface. The result confirmed that the poly-A successfully coated at the surface of the electrode. In particular, the addition of poly-A reduced the water contact angle from 45.8 to 23.4°, suggesting a significant increase in hydrophilicity at the electrode interface. The increase in hydrophilicity helped form a tightly bound water layer near the electrode interface by the interaction between hydrogen bonds and water molecules, which provided a physical barrier to hinder protein proximity and adsorption.[19] Therefore, the addition of poly-A improved the anti-non-specific adsorption ability on the electrode interface.

The immobilization of DNA on the electrode surface was characterized by electrostatic adsorption between the MB and DNA phosphoric acid backbone (Figure 1B). Some MB adsorbed at the electrode interface without DNA; thus, no obvious redox peak was observed for GE and HT assembled electrodes (curves a and b). When the Cp was immobilized at the electrode interface, MB adsorbed on Cp, resulting in a significant redox current (curve c). Due to the weak affinity between adenine and MB,[20] the signal was barely increased with the addition of poly-A (curve d). It is worth mentioning that compared to the electrode modified only with HT, the immobilization of Cp and the addition of poly-A did not observably change the charging current (as illustrated by the double-headed arrow in Figure 1B, the charging current is defined by the sum of the absolute values of the oxidation current and the reduction current at 0 V), indicating that the tight packing of HT on the surface was unaffected by the assembly of Cp and poly-A.[3] Meanwhile, electrochemical impedance spectroscopy (EIS) was used to characterize the assembly process, and the results in Figure S4 show the successful assembly of HT and poly-A.

To further confirm that the addition of poly-A hardly affects the assembly of HT, density functional theory (DFT) calculations were performed to compare the interaction between Au and adenine or HT (details shown in Table S2 and its explanatory note). DFT results revealed that HT can tightly bind the Au atom via forming an Au−S bond with a Wiberg bond index of 0.433, resulting in a high binding energy of 0.43 eV (Figure 1C). Although adenine can also interact with the Au atom via one of its nitrogen atoms, the Wiberg bond index of the formed Au−N bond was only 0.164 and the binding energy was as small as 0.12 eV (Figure 1D), which were both smaller than those of the HT−Au complex (Table S2). These results demonstrate that the interaction between HT and Au was much stronger than that between poly-A and Au, validating that the stable assembly of HT on GE will not be replaced by the addition of poly-A. This statement was also verified by calculating the surface coverage density of HT with and without poly-A. As shown in Figure S5, the addition of poly-A did not change the reductive desorption peak area, and the surface coverage density of HT and HT−poly-A was 9.38×10^{-9} and 9.44×10^{-9} mol/cm^2, respectively. This result suggested that the addition of poly-A did not affect the surface coverage density of HT, which was consistent with the DFT calculation results.

Feasibility of Hybridization Detection on the HT−Poly-A Assembled Electrode. The hybridization of DNA at the electrode interface is fundamental to electrochemical DNA sensors. Therefore, to investigate the feasibility of DNA hybridization at the HT assembled electrode interface, cholesteryl-modified Cp was first immobilized at the HT assembled electrode interface, and then, the MB-modified

https://doi.org/10.1021/acs.analchem.2c00069
Anal. Chem. 2022, 94, 5382−5391

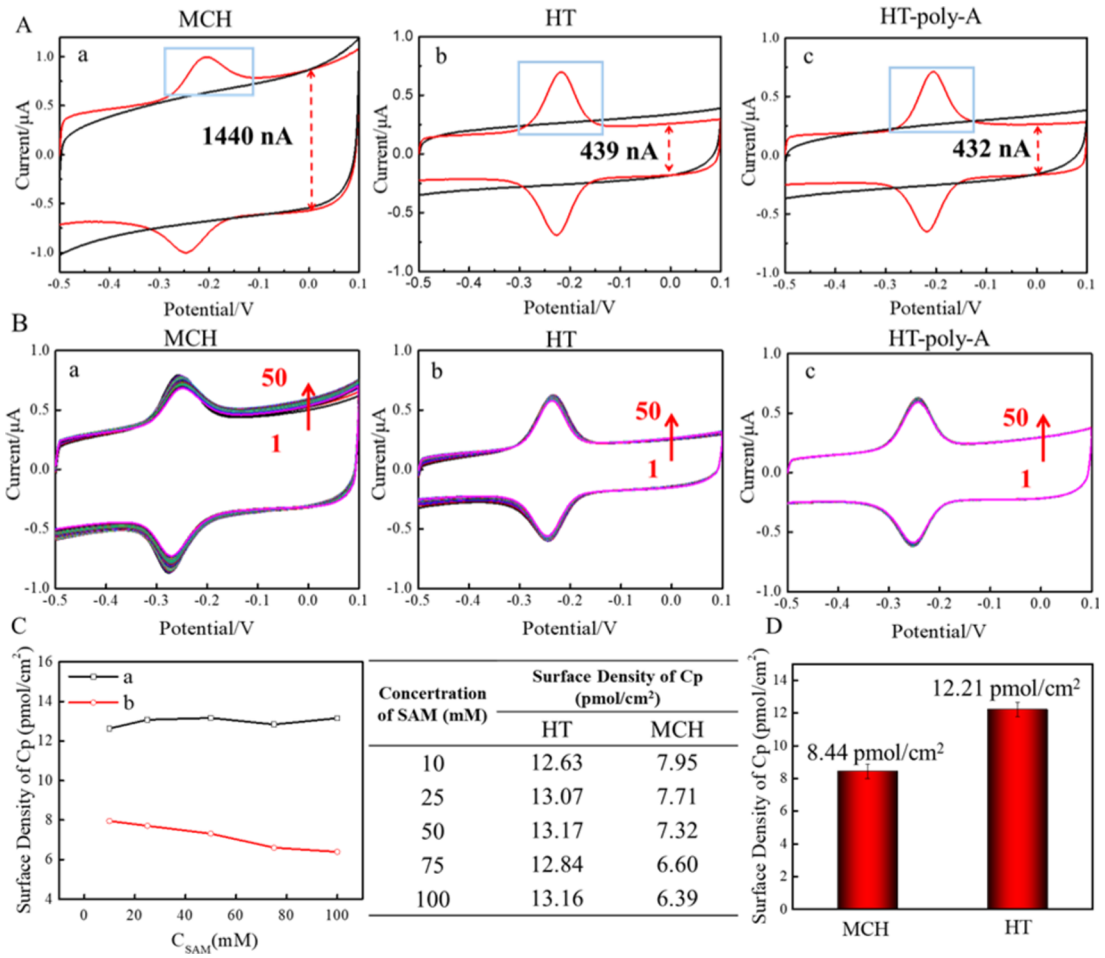

Concertration of SAM (mM)	Surface Density of Cp (pmol/cm²)	
	HT	MCH
10	12.63	7.95
25	13.07	7.71
50	13.17	7.32
75	12.84	6.60
100	13.16	6.39

Figure 2. (A) Charging current and (B) stability of different assembled electrodes: (a) GE/Cp/MCH/Sp-MB, (b) GE/HT/Cp/Sp-MB, and (c) GE/HT/Cp/poly-A/Sp-MB. To measure stability, the signal response was detected in PBS, and the next scan was performed immediately after the completion of the first CV scan, for a total of 50 times. (C) Comparison of competition between SAM and DNA probes. The effects of different concentrations (10, 25, 50, 75, and 100 mM) of HT and MCH on the Cp were demonstrated: (a) GE/HT/MB-Cp and (b) GE/MB-Cp/MCH. The detailed values of surface densities of Cp are listed in the right table. (D) Calculated assembly density of Cp on the electrode modified with 5 mM MCH and HT.

DNA was used as the signal probe (Sp-MB) to hybridize with Cp (Figure S6A). The modified MB was close to the electrode interface to obtain a significant redox current. As a control, MCH assembled electrodes were prepared according to the previous works (Figure S6B). As shown in Figure S7, when only Cp was immobilized on the HT assembled electrode, the redox peak was not observed (curve a). After hybridization of Cp and Sp-MB, HT (curve b), HT−poly-A (curve c), and MCH (curve d) assembled electrodes all showed symmetrical redox peaks, suggesting the successful hybridization of Sp-MB and Cp on all assembled electrodes.

Importantly, HT and HT−poly-A assembled electrodes showed a smaller charging current than MCH. It is because the tightly packed hydrophobic monolayer decreased the water penetration, leading to a decrease in the double-layer capacitance, thereby reducing the current required for the charging of the double layer.[21] To this end, we calculated the charging current of the electrode at a potential of 0 V (Figure 2A). Obviously, the charging current observed in HT assembled electrodes (439 nA, Figure 2Ab) was 1 order of magnitude smaller than that of MCH assembled electrodes (1440 nA, Figure 2Aa). The tight packing of HT on the surface was not influenced by the attachment of poly-A as there was barely any change in the charging current (432 nA, Figure 2Ac). Moreover, we observed that the assembly of HT significantly enhanced signal outputs, which were manifested as a larger area under the MB oxidation peaks in CV (the blue box illustrated in Figure 2A) and a higher peak current (I_p). As shown in Figure S8A, the average I_p of HT and HT−poly-A were 430 and 439 nA, which were larger than that of MCH (357 nA). The increase in I_p is associated with the amphiphilic electrode interface. The hydrophobic HT SAM can avoid the hydrophilic DNA lodging on the gold surface, ensuring the efficiency of DNA hybridization on the electrode. In addition, the value of the total current in CV is equal to the sum of the charging current and the faradaic current.[3] As a result, the decrease in the charging current makes it easier to distinguish the faradaic current reported by the surface bound redox probe, leading to a higher SNR detection. Therefore, we compared SNRs of different assembled electrodes by calculating the ratio of the I_p in the presence and absence of Sp-MB in CV curves. On account of the the decrease in the charging current, the SNR increased from 16 for MCH to 47 for HT and 48 for HT−poly-A (Figure S8B), suggesting that HT and HT−poly-A obtained a better SNR than MCH as a self-assembled layer.

https://doi.org/10.1021/acs.analchem.2c00069
Anal. Chem. 2022, 94, 5382−5391

Stability of Hybridization Detection on the HT−Poly-A Assembled Electrode. The tightly packed assembly layer made the HT assembled electrode more stable than the MCH assembled electrode under continuous voltammetric interrogation. As shown in Figure S9, histogram a, after 50 consecutive CV scans, the I_p of the MCH assembled electrode was reduced by 26.32%, and a significant increase in charging current is observed in Figure 2B, curve a. The results suggested that the MCH assembled electrode showed progressive desorption during continuous electrochemical interrogation, which induced the decrease in the redox current and the increase in the charging current.[3] A possible explanation for this might be that, in a water solution, the hydrophilic MCH is covered by water, and these water layers may lead to a disruption of the monolayer packing by the interaction of water in the hydrocarbon lattice.[18] However, as observed in Figure S9, histograms b and c, the HT and HT−poly-A assembled electrodes were reduced by only 7.75 and 7.47% after 50 consecutive CV scans, suggesting better stability than that of the MCH assembled electrode. Furthermore, no obvious increase in the charging current of both HT and HT−poly-A assembled electrode was observed (Figure 2B, curves b and c). This may be due to the fact that the hydrophobic tight monolayer can effectively resist the progressive degradation of the monolayer caused by water permeation during continuous electrochemical interrogation.[3] In addition, we fabricated the assembled electrode and placed them in 4 °C for 1 week to investigate the temporal stability. As shown in Figure S10, after a week, the I_p of the MCH assembled electrode was reduced by 36.25%, whereas the HT and HT−poly-A assembled electrodes still showed better stability as the signals were reduced by 7.12 and 5.35% only. Therefore, in contrast to the MCH assembled electrode, HT and HT−poly-A assembled electrodes have better stability, possessing great potential in long-term biosensing.

Reproducibility of Hybridization Detection on the HT−Poly-A Assembled Electrode. The reproducibility of detection is crucial to electrochemical biosensors, which directly affects the accuracy of detection results. To this end, we compared the detection reproducibility of HT−poly-A and MCH assembled electrodes by recording the current signal of Sp-MB captured in 5 different electrodes. As shown in Figure S11, the relative standard deviation (RSD) of HT−poly-A assembled electrode was 3.81% (Figure S11A), lesser than 9.81% for MCH (Figure S11B), suggesting a better reproducibility of detection. The low reproducibility of the MCH assembled electrode may be related to the competition between MCH and thiol-modified DNA at the GE. Some studies have revealed that the inter-helical interactions in thiol-modified DNA will cause the inhomogeneous distribution on the electrode, and MCH competitively displacing the DNA will further intensify the heterogeneity.[22] This inhomogeneous assembly is especially problematic for biosensing because it may cause large detection errors and poor reproducibility.[23] In contrast to the conventional preparations of DNA monolayers by connecting the thiol-modified DNA directly to GE, the cholesteryl-modified DNA was immobilized to the electrode by hydrophobic interaction with HT, bringing the electrode interface in indirect contact with DNA. Thus, we assumed that this immobilization method reduced the competition between DNA and SAM, ensuring good reproducibility. To validate the hypothesis, the effects of different immobilization methods on the DNA probe on the electrode surface were investigated by calculating the density of MB-modified Cp on the electrode surface (details shown in Figure S12A−C).[3] As expected, the assembly of HT did not influence the immobilization of Cp because the surface density of Cp was almost constant with the increase in the HT concentration (Figure 2C, curve a). In contrast, the surface density of Cp on the MCH assembled electrode decreased from 7.95 to 6.39 pmol/cm^2 with the increase in the MCH concentration, suggesting the competition between MCH and the thiol-terminated Cp (Figure 2C, curve b). To further evaluate the effect of different immobilization methods on the Cp assembly efficiency, the surface density of Cp on the electrode at the same concentrations (5 mM) of SAM was calculated. As shown in Figure 2D, the surface density of Cp on the HT assembled electrode was 12.21 pmol/cm^2, which was higher than that of the MCH assembled electrode (8.44 pmol/cm^2), suggesting a better probe assembly efficiency for the HT assembled electrode. Taken together, these results demonstrated that the HT−poly-A assembled electrode had a high SNR and great stability and reproducibility, setting an excellent example for obtaining better sensing performance in electrochemical biosensors.

Anti-Fouling Ability of Hybridization Detection on the HT−Poly-A Assembled Electrode. Inevitably, HT assembled electrodes are ineffective at resisting the nonspecific adsorption of proteins due to their hydrophobicity,[3] despite their excellent stability, reproducibility, and SNR. We believed that further blocking the electrode with poly-A can compensate for this shortcoming without affecting the electron transport.[11] To this end, we conducted a visual evaluation to compare the anti-fouling ability of different electrodes. All electrodes were immersed in fluorescein isothiocyanate labeled BSA (FITC-BSA) (10 mg·mL^{-1}) for 2 h and washed before analysis. As displayed in Figure S13Aa, the interface of GE had a bright green fluorescence. Although the assembly of MCH or HT reduced the adsorption of BSA significantly (Figure S13Ab,c), a small volume of green fluorescence could still be observed. However, the HT−poly-A assembled electrode showed a better anti-fouling ability with barely any observable green fluorescence (Figure S13Ad), proving that the HT−poly-A assembled electrode has the potential for sensing in complex biological fluids.

To further investigate the resistance of the HT−poly-A self-assembled layer to protein adsorption, the electrodes were incubated in 50% human serum for 1 h to directly capture the Sp-MB in it (Figure S13B), and the Sp-MB captured in PBS was used as the control. As shown in Figure S13C, the biofouling of various proteins in serum severely hindered the electron transfer at the electrode interface, resulting in a significant decrease in the peak of redox of the MCH and HT assembled electrode, which maintained only 36.65 and 35.57% of the original current, respectively (Figure S13D). The addition of poly-A improved the anti-fouling ability of the HT assembled electrode, exhibiting a distinct redox peak and maintaining 63.16% of the original current. Therefore, we envision that this design of the HT−poly-A assembled layer can be employed as a universal strategy to improve the performance of electrochemical sensing.

Tightly Packed HT Assembled Layer for Application in Electrocatalytic Reaction-Based Electrochemical Biosensors. We further demonstrate the advantage of tightly packed assembly layers for hybridization detection using electrocatalytic signal amplification reaction strategy. The

https://doi.org/10.1021/acs.analchem.2c00069
Anal. Chem. 2022, 94, 5382−5391

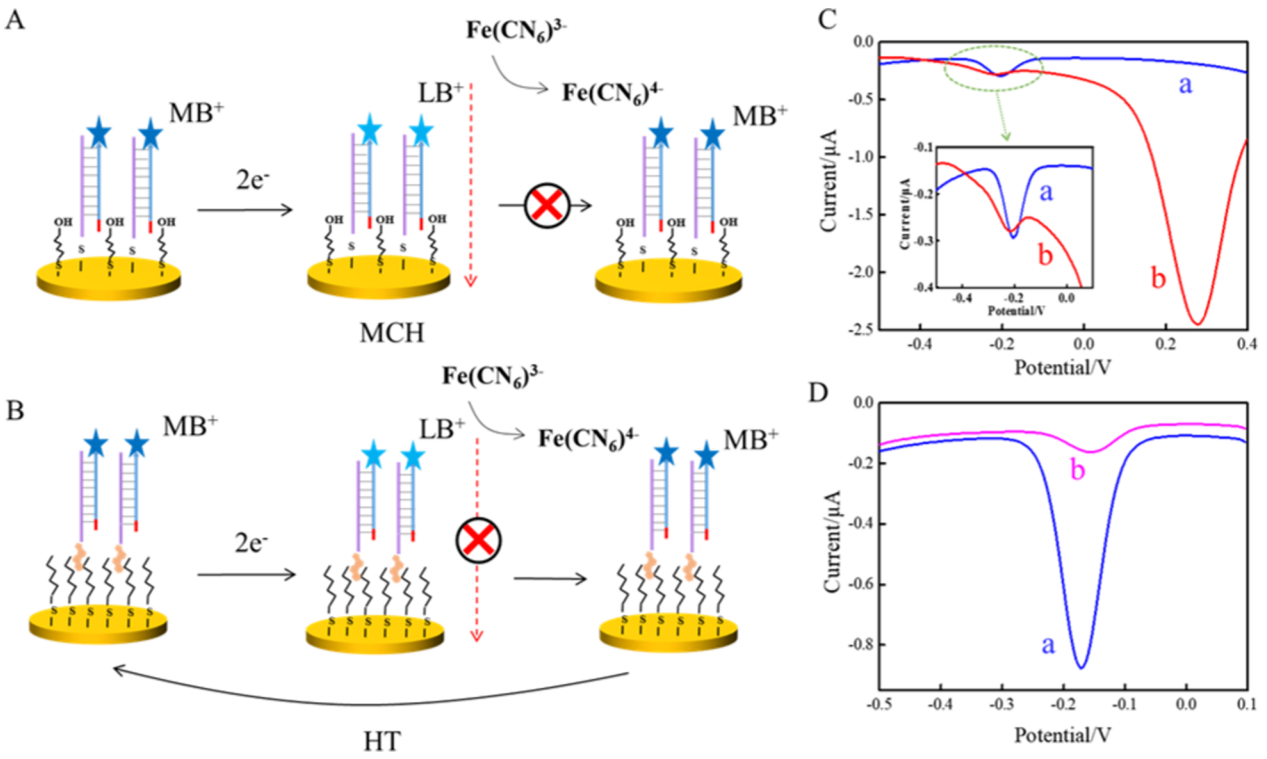

Figure 3. Schematic diagram of the electrocatalytic reaction performed in (A) GE/Cp/MCH/Sp-MB and (B) GE/HT/Cp/Sp-MB. (C) SWVs of electrocatalytic reduction of different assembled electrodes: (a) GE/HT/Cp/Sp-MB and (b) GE/Cp/MCH/Sp-MB. These experiments were performed in 1× PBS containing 2 mM $[Fe(CN)_6]^{3-}$. (D) Signal response comparison of GE/HT/Cp/Sp-MB in PBS (a) with 2 mM $[Fe(CN)_6]^{3-}$ and (b) without $[Fe(CN)_6]^{3-}$.

mechanism of the reaction is shown in Figure 3. Electrons flow from the electrode interface to the MB^+ bound at the top of the DNA via the DNA helical mediation, generating leucomethylene blue (LB^+). The reduction of $[Fe(CN)_6]^{3-}$ with LB^+ in the solution causes more electrons to flow to MB^+, and the catalytic cycles continues to produce the catalytic current. In classical electrocatalytic reactions,[24] to avoid the interference of the electrocatalytic reduction reaction by the electron transfer between $[Fe(CN)_6]^{3-}$ and electrode interface, $[Fe(CN)_6]^{3-}$ is required to be away from the electrode surface by the electrostatic repulsion of the ultrahigh density packing of the DNA probe (100 μM) and MB^+ is required to bind to the top of the DNA probe. However, the tight packing of DNA at the electrode interface makes it difficult to regulate the spacing between DNAs, which limits the application of this reaction in electrochemical biosensors based on DNA configuration change.[25] Although some works used 2-azidododecane-1-thiol and 11-mercapto-undecylphosphoric acid to block the electrode surface for avoiding the interference of $[Fe(CN)_6]^{3-}$,[26] the long alkyl chain may passivate the electrode, leading to low sensitivity.[27] In a traditional MCH assembled electrode, the exposed gold sites from the imperfect MCH blocking provided a channel for electron transfer between $[Fe(CN)_6]^{3-}$ and the electrode interface (Figure 3A). Therefore, in CV scanning results, a significant redox peak was observed for the MCH assembled electrode in the $[Fe(CN)_6]^{3-}$ solution (Figure S14A). However, interestingly, our tightly packed HT SAM can effectively inhibit the electrochemical redox reaction between the electrode and $[Fe(CN)_6]^{3-}$ without the need for a high-density DNA assembled layer (Figure 3B). As a result, no redox peak of $[Fe(CN)_6]^{3-}$ at the HT assembled electrode was observed (Figure S14B). When the electrocatalytic reaction occurred, as shown in Figure 3C, even with low density of dsDNA (0.1 μM) on the electrode, the HT assembled electrode showed a large catalytic current (curve a). However, the catalytic current of the MCH assembled electrode was significantly less than that of HT, and a large current produced by the reaction between $[Fe(CN)_6]^{3-}$ and the electrode interface was observed (curve b). This demonstrated that the inhibited redox reaction between the electrode and $[Fe(CN)_6]^{3-}$ made it easier for the HT assembled electrode to implement electrocatalytic reaction than the MCH assembled electrode. Also, as shown in Figure 3D, the MB current response showed a 10-fold increase in $[Fe(CN)_6]^{3-}$ (curve a) than in the PBS buffer (curve b), meaning that this electrocatalytic reaction can effectively amplify the current of MB in the HT assembled electrode. Overall, these results indicated that the electrocatalytic reaction based on the HT assembled electrode had great application prospect in DNA configuration change-based electrochemical biosensors.

Dual-Signal Amplification Biosensor for the Detection of Exosomal miR-21. Enzyme-assisted nucleic acid amplification reaction (EAAR) has been widely used for the fabrication of DNA electrochemical biosensors due to its high amplification efficiency. However, the use of enzymes is a double-edged sword, which effectively improves the sensitivity but also leads to the non-specific adsorption of electrodes. In this context, we attempted to use the HT−poly-A self-assembled electrode to perform EAAR to overcome this issue.

Principle of Dual-Amplification Biosensor for the Detection of Exosomal miR-21. As shown in Figure 4, this biosensor was composed of the assembly of HT−poly-A, the first signal amplification step (FDSDR), and the second signal

https://doi.org/10.1021/acs.analchem.2c00069
Anal. Chem. 2022, 94, 5382−5391

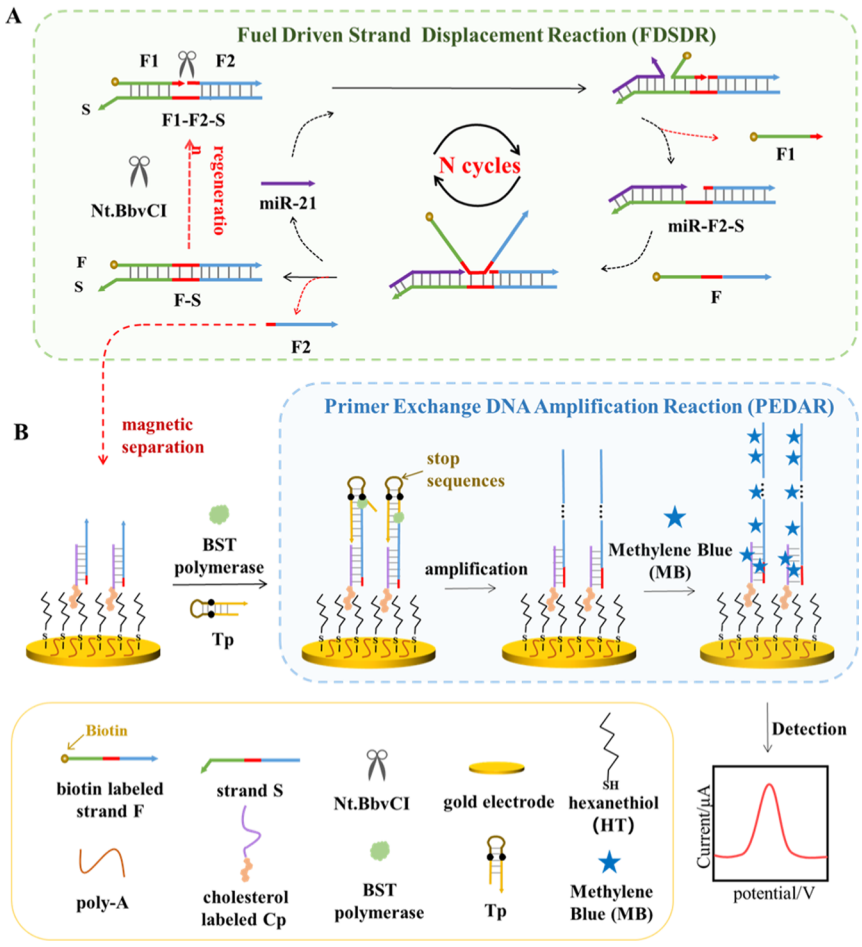

Figure 4. Schematic illustration of a dual-signal amplification electrochemical sensor. Principle of (A) FDSDR and (B) PEDAR.

amplification step (PEDAR). In FDSDR, miR-21 triggered cascade amplification by strand displacement (Figures 4A, S15A). FDSDR achieved higher cycle efficiency than classical cascade displacement[28] reactions by reasonably recovering waste strands (Figure S15B) and produced a large amount of F2 strands, which were then captured on the electrode to initiate PEDAR (Figures 4B, S16). PEDAR, an isothermal amplification technique, is a one-step amplification of single-stranded DNA (ssDNA).[16] A large number of long ssDNAs were produced on the electrode to recruit MB by electrostatic adsorption, which produced an amplified electrochemical signal.

Characterization of FDSDR and PEDAR. To characterize the amplification processes, fluorescence spectroscopy, polyacrylamide gel electrophoresis (PAGE), and CV were performed. The fluorophore and the quencher were separated in the presence of miR-21 by strand displacement, resulting in an enhancement of fluorescence (Figure S17A,B). In the PAGE image (Figure S17C), the band of F2 was observed in lane 7 when FDSDR was triggered. Also, the produced F2 resulted in a significant increase in the redox peak (Figure S19, curve e). When PEDAR was triggered, long ssDNA was produced and showed in lane 3 in the PAGE image (Figure S18) and further increased the redox current (Figure S19, curve f).

Performance of the Electrochemical Biosensor. To achieve the best detection performance, the amount of streptavidin magnetic beads, the concentration of F and Nt.BbvCI enzyme, and the reaction time of different steps were optimized, respectively (Figures S20, S21). Under the optimum reaction conditions, the performance of the proposed dual amplification biosensor was investigated.

The sensitivity of the sensor was evaluated by SWV. With the increase in miR-21 concentration, the detected current signal of SWV increased (Figure 5A) and approached saturation at 50 nM (Figure S22). The dynamic range of detection was from 100.00 aM to 1.00 nM. The concentration of miR-21 showed a good linear relationship with the current signal and the limit of detection (LOD) of the proposed biosensor was calculated as 1.46 aM based on the 3σ/slope rule (Figure 5B).[29] Compared to other recently reported miRNA sensors, the proposed sensor had a lower LOD (Table S3).[2,30−38] The dual signal amplification steps ensured the sensitivity of this sensor, showing a great potential for tumor marker-based diagnosis. The specificity of the proposed biosensor was evaluated with base-mismatched sequences and homologous miRNAs as interference agents. As shown in Figure 5C, the addition of miR-21 showed a large current, while the currents of base-mismatched sequences and homologous miRNAs sequences were very small, which validated the favorable selectivity of this sensor. To monitor the stability of this biosensor over time, we stored the fabricated biosensors at 4 °C for 7 days and reevaluated current responses after storage. As expected, the current response of the electrodes stored after 7 days decreased by only 2.74% compared to the initial current on the first day

https://doi.org/10.1021/acs.analchem.2c00069
Anal. Chem. 2022, 94, 5382−5391

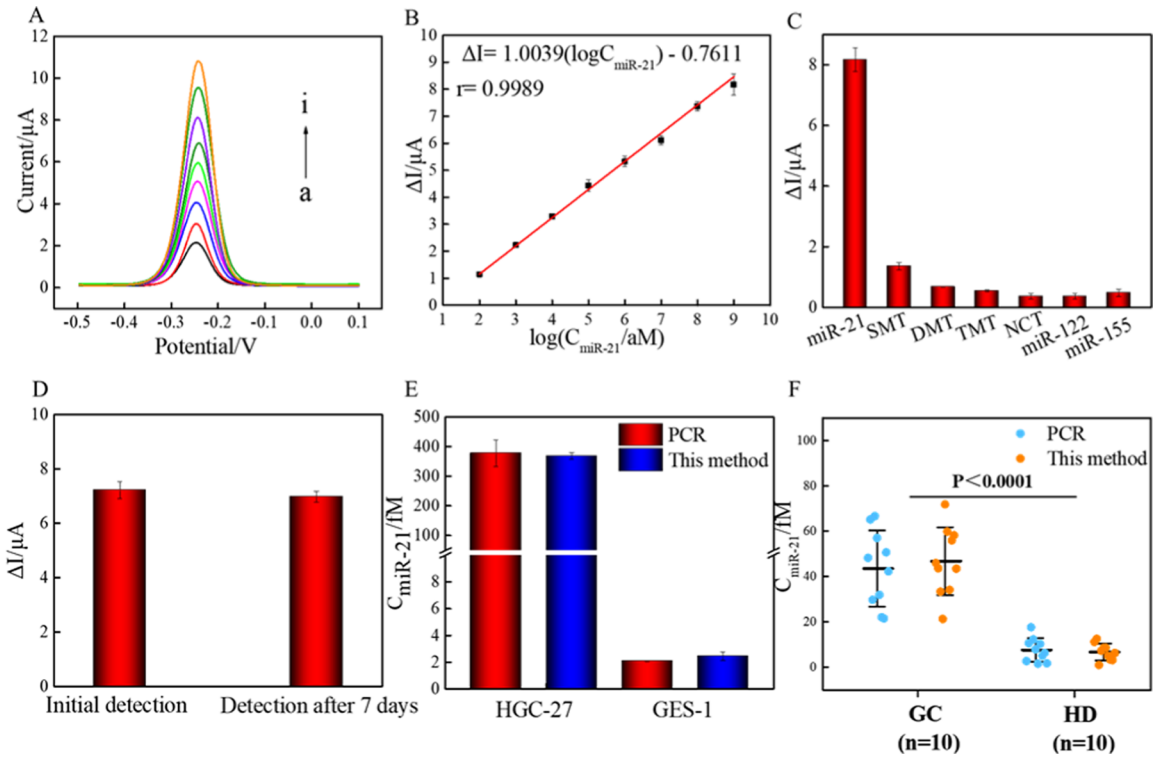

Figure 5. (A) Current signals of different concentrations of miR-21 with the proposed biosensor. Concentrations of miR-21 from (a–i): 0, 10^2, 10^3, 10^4, 10^5, 10^6, 10^7, 10^8, and 10^9 aM. (B) Calibration curve fitted by the current change (ΔI) before and after the addition of miR-21 and the logarithm of concentration of miR-21 (lg C_{miR-21}). (C) Selectivity analysis of the proposed biosensor toward miR-21, mismatched miR-21 (SMT: single-base mismatched target; DMT: double-base mismatched target; TMT: three-base mismatched target; NCT: non-complementary target) and homologous miRNAs (miR-122, miR-155) at the same concentration of 1 nM. (D) Temporal stability of the proposed biosensor. (E) Detection of HGC-27 cell and GES-1 cell derived exosomal miR-21 by RT-qPCR and the proposed electrochemical biosensor. (F) Detection of miR-21 content in human serum exosomes isolated from patients with gastric cancer (GC) and healthy donors (HD).

(Figure 5D). The anti-fouling ability of this biosensor was tested by the detection of miRNA in the serum. The miR-21 was diluted with serum and PBS and then measured with the proposed biosensor. Figure S23 shows that the proposed sensor still maintained a good current response in human serum, suggesting its great performance for sample detection in biofluids. Notably, the RSD of five times detection in serum and PBS was lesser than 4.5%, indicating the good reproducibility of the proposed biosensor. In conclusion, the proposed biosensor, with high sensitivity and excellent specificity and selectivity, is considered as a powerful tool for the detection of exosomal miRNAs.

Detection of Exosomal miR-21 of Cell and Serum Samples. Exosomes extracted from HGC-27 cells were used to evaluate the potential of the proposed sensor for the clinical sample detection. The isolated exosomes showed a disk-like morphology with a diameter of 30–150 nm and expressed CD9, CD63, and TSG101 proteins (Figure S24). These results were consistent with previous reports.[39] Subsequently, we used the proposed electrochemical biosensor to assay the abundance of exosomal miR-21 from HGC-27 cells and GES-1 cells. As expected, exosomal miR-21 of HGC-27 cells showed a higher abundance than that of GES-1 cells (Figure 5E), which indicated that the biosensor can distinguish HGC-27 cells and GES-1 cells to some extent. The above detection results were consistent with RT-PCR results.

Finally, we evaluated the performance of detecting exosomal miR-21 in human serum for cancer diagnosis. We collected serum samples from 10 untreated patients with GC for detecting exosomal miR-21, and serum samples from 10 HD were used as controls. The results in Figure 5F indicate that all of the GC-positive patients showed high expression of exosomal miR-21, which was significantly different from that of HD (double-tailed *t*-test analysis, $p < 0.0001$). Taken together, we believe that the proposed electrochemical biosensor has practical application value and potential in the field of early cancer diagnosis.

CONCLUSIONS

In this work, we reported an HT–poly-A self-assembled layer to improve the SNR, reproducibility, and stability of electrochemical detection as well as to avoid non-specific adsorption on electrodes. This self-assembly layer showed the following advantages: (1) the tight packing of HT at the electrode interface resulted in a better stability and high SNR electrochemical detection and can inhibit the electrochemical redox between $[Fe(CN)_6]^{3-}$ and the electrode, making the electrocatalytic reaction easy to realize without the need for high assembly density of the DNA probe; (2) the hydrophobic interaction between HT and cholesterol limited the shedding of the DNA probe on the electrode interface, improving the assembly efficiency of DNA and the reproducibility of the detection; (3) the introduction of poly-A further enhanced the anti-fouling capability of the electrode, making it possible for electrochemical sensing in complex biological fluids. As an alternative to MCH SAM, the HT–poly-A self-assembled layer is simple and universal. The dual signal amplification in this biosensor achieved an LOD of 1.46 aM and a dynamic range

https://doi.org/10.1021/acs.analchem.2c00069
Anal. Chem. 2022, 94, 5382–5391

from 100.00 aM to 1.00 nM. Overall, our biosensor has demonstrated the ability to detect miR-21 in GC exosomes in clinical samples. More research can be done to further improve its performance. For example, the length of poly-A can be optimized to achieve higher fouling resistance; combining electrocatalytic reaction and enzyme-assisted signal amplification may achieve higher sensitivity. In short, we envision that the proposed strategy may be finely tuned and exploited to gain further improvement in electrochemical biosensors for the early screening and diagnosis of cancer.

■ ASSOCIATED CONTENT

Supporting Information

The Supporting Information is available free of charge at https://pubs.acs.org/doi/10.1021/acs.analchem.2c00069.

Cell culture and exosome extraction isolation; exosome RNA extraction; characterization of SAM assembly; calculation of the covering density of SAM; EIS characterization of different assembly processes; SNR, stability, reproducibility, anti-fouling ability, and DNA surface density of different assembled electrodes; schematic diagram of the classical strand displacement reaction and PEDAR; characterization of FDSDR and PEDAR; feasibility of the proposed biosensor; optimization of experimental parameters; the anti-fouling ability of the proposed biosensor; characterization of exosome; oligonucleotide sequences; the details of DFT calculations; and the reported different biosensors for detection of exosomal miRNAs in recent years (PDF)

■ AUTHOR INFORMATION

Corresponding Authors

Xi Zhang − *Department of Clinical Pharmacy, The School of Pharmacy, Fujian Medical University, Fuzhou 350122, P. R. China*; Email: xz@fjmu.edu.cn

Jing Zhang − *College of Life Sciences, Fujian Agriculture and Forestry University, Fuzhou 350002, P.R. China*; Email: 1601225385@qq.com

Jinghua Chen − *Department of Pharmaceutical Analysis, The School of Pharmacy and Fujian Key Laboratory of Drug Target Discovery and Structural and Functional Research, The School of Pharmacy, Fujian Medical University, Fuzhou 350122, P.R. China*; orcid.org/0000-0001-8718-0232; Email: cjh_huaxue@126.com

Authors

Guanyu Chen − *Department of Pharmaceutical Analysis, The School of Pharmacy and Fujian Key Laboratory of Drug Target Discovery and Structural and Functional Research, The School of Pharmacy, Fujian Medical University, Fuzhou 350122, P.R. China*

Wenqian Chen − *Department of Pharmaceutical Analysis, The School of Pharmacy and Fujian Key Laboratory of Drug Target Discovery and Structural and Functional Research, The School of Pharmacy, Fujian Medical University, Fuzhou 350122, P.R. China*

Lilan Xu − *Department of Pharmaceutical Analysis, The School of Pharmacy and Fujian Key Laboratory of Drug Target Discovery and Structural and Functional Research, The School of Pharmacy, Fujian Medical University, Fuzhou 350122, P.R. China*

Huixuan Jin − *College of Life Sciences, Fujian Agriculture and Forestry University, Fuzhou 350002, P.R. China*

Weiming Sun − *Department of Pharmaceutical Analysis, The School of Pharmacy and Fujian Key Laboratory of Drug Target Discovery and Structural and Functional Research, The School of Pharmacy, Fujian Medical University, Fuzhou 350122, P.R. China*; orcid.org/0000-0002-9882-0511

Jianming Lan − *Department of Pharmaceutical Analysis, The School of Pharmacy and Fujian Key Laboratory of Drug Target Discovery and Structural and Functional Research, The School of Pharmacy, Fujian Medical University, Fuzhou 350122, P.R. China*

Fang Wu − *Department of Pharmaceutical Analysis, The School of Pharmacy and Fujian Key Laboratory of Drug Target Discovery and Structural and Functional Research, The School of Pharmacy, Fujian Medical University, Fuzhou 350122, P.R. China*

Complete contact information is available at: https://pubs.acs.org/10.1021/acs.analchem.2c00069

Author Contributions

⊥G.C. and W.C. contributed equally.

Notes

The authors declare no competing financial interest.

■ ACKNOWLEDGMENTS

The authors gratefully acknowledge the financial support of National Natural Science Foundation of China (21874019), the Fujian Science and Technology Innovation Joint Found Project (2019Y9008), the Science and Technology Plan Guided Project of the Fujian Provincial Science and Technology Department (2020Y0022), the Natural Science Foundation of Fujian Province (nos 2019J01681, 2020J01545), and the United Fujian Provincial Health and Education Project for Tackling the Key Research, China (WKJ2016-2-30). We would like to thank Sishi Chen, who is from the Public Technology Service Center (Fujian Medical University), for technical assistance.

■ REFERENCES

(1) Wang, L.-L.; Chen, W.-Q.; Wang, Y.-R.; Zeng, L.-P.; Chen, T.-T.; Chen, G.-Y.; Chen, J.-H. *Biosens. Bioelectron.* **2020**, *169*, 112555.
(2) Guo, Q.; Yu, Y.; Zhang, H.; Cai, C.; Shen, Q. *Anal. Chem.* **2020**, *92*, 5302−5310.
(3) Shaver, A.; Curtis, S. D.; Arroyo-Currás, N. *ACS Appl. Mater. Interfaces* **2020**, *12*, 11214−11223.
(4) Li, S.; Wang, Y.; Zhang, Z.; Wang, Y.; Li, H.; Xia, F. *Anal. Chem.* **2021**, *93*, 5849−5855.
(5) Jolly, P.; Miodek, A.; Yang, D.-K.; Chen, L.-C.; Lloyd, M. D.; Estrela, P. *ACS Sens.* **2016**, *1*, 1308−1314.
(6) Feng, T.; Ji, W.; Zhang, Y.; Wu, F.; Tang, Q.; Wei, H.; Mao, L.; Zhang, M. *Angew. Chem., Int. Ed. Engl.* **2020**, *59*, 23445−23449.
(7) Sabaté del Río, J.; Henry, O. Y. F.; Jolly, P.; Ingber, D. E. *Nat. Nanotechnol.* **2019**, *14*, 1143−1149.
(8) Han, R.; Wang, G.; Xu, Z.; Zhang, L.; Li, Q.; Han, Y.; Luo, X. *Biosens. Bioelectron.* **2020**, *164*, 112317.
(9) Bui-Thi-Tuyet, V.; Trippé-Allard, G.; Ghilane, J.; Randriamahazaka, H. *ACS Appl. Mater. Interfaces* **2016**, *8*, 28316−28324.
(10) Vericat, C.; Vela, M. E.; Benitez, G.; Carro, P.; Salvarezza, R. C. *Chem. Soc. Rev.* **2010**, *39*, 1805−1834.
(11) Traynor, S. M.; Wang, G. A.; Pandey, R.; Li, F.; Soleymani, L. *Angew. Chem., Int. Ed.* **2020**, *59*, 22617−22622.
(12) Salehi, M.; Sharifi, M. *J. Cell. Physiol.* **2018**, *233*, 6370−6380.

(13) Kulkarni, B.; Kirave, P.; Gondaliya, P.; Jash, K.; Jain, A.; Tekade, R. K.; Kalia, K. *Drug Discov. Today* **2019**, *24*, 2058−2067.
(14) Lao, R.; Song, S.; Wu, H.; Wang, L.; Zhang, Z.; He, L.; Fan, C. *Anal. Chem.* **2005**, *77*, 6475−6480.
(15) Zhang, C.; Wang, Z.; Liu, Y.; Yang, J.; Zhang, X.; Li, Y.; Pan, L.; Ke, Y.; Yan, H. *J. Am. Chem. Soc.* **2019**, *141*, 17189−17197.
(16) Kishi, J. Y.; Schaus, T. E.; Gopalkrishnan, N.; Xuan, F.; Yin, P. *Nat. Chem.* **2018**, *10*, 155−164.
(17) Makaraviciute, A.; Xu, X.; Nyholm, L.; Zhang, Z. *ACS Appl. Mater. Interfaces* **2017**, *9*, 26610−26621.
(18) Poirier, G. E.; Pylant, E. D.; White, J. M. *J. Chem. Phys.* **1996**, *104*, 7325−7328.
(19) Chen, S.; Yu, F.; Yu, Q.; He, Y.; Jiang, S. *Langmuir* **2006**, *22*, 8186−8191.
(20) Atherton, S. J.; Harriman, A. *J. Am. Chem. Soc.* **1993**, *115*, 1816−1822.
(21) Chidsey, C. E. D.; Loiacono, D. N. *Langmuir* **1990**, *6*, 682−691.
(22) Murphy, J. N.; Cheng, A. K. H.; Yu, H.-Z.; Bizzotto, D. *J. Am. Chem. Soc.* **2009**, *131*, 4042−4050.
(23) Nano, A.; Furst, A. L.; Hill, M. G.; Barton, J. K. *J. Am. Chem. Soc.* **2021**, *143*, 11631−11640.
(24) Boon, E. M.; Ceres, D. M.; Drummond, T. G.; Hill, M. G.; Barton, J. K. *Nat. Biotechnol.* **2000**, *18*, 1096−1100.
(25) Wang, C.; Liu, L.; Zhao, Q. *ACS Sens.* **2020**, *5*, 3246−3253.
(26) Furst, A.; Landefeld, S.; Hill, M. G.; Barton, J. K. *J. Am. Chem. Soc.* **2013**, *135*, 19099−19102.
(27) Wang, L.; Polyansky, D. E.; Concepcion, J. J. *J. Am. Chem. Soc.* **2019**, *141*, 8020−8024.
(28) Xia, Y.; Wang, L.; Li, J.; Chen, X.; Lan, J.; Yan, A.; Lei, Y.; Yang, S.; Yang, H.; Chen, J. *Anal. Chem.* **2018**, *90*, 8969−8976.
(29) Chai, S. Q.; Lv, W. Y.; He, J. H.; Li, Y. F.; Zou, H. Y.; Li, C. M.; Huang, C. Z. *Anal. Chem.* **2021**, *93*, 14545−14551.
(30) Zhan, X.; Yang, S.; Huang, G.; Yang, L.; Zhang, Y.; Tian, H.; Xie, F.; Lamy de la Chapelle, M.; Yang, X.; Fu, W. *Biosens. Bioelectron.* **2021**, *188*, 113314.
(31) Xia, Y.; Chen, T.; Zhang, L.; Zhang, X.; Shi, W.; Chen, G.; Chen, W.; Lan, J.; Li, C.; Sun, W.; Chen, J. *Biosens. Bioelectron.* **2021**, *173*, 112834.
(32) Liu, P.; Qian, X.; Li, X.; Fan, L.; Li, X.; Cui, D.; Yan, Y. *ACS Appl. Mater. Interfaces* **2020**, *12*, 45648−45656.
(33) Miao, P.; Tang, Y. *Anal. Chem.* **2020**, *92*, 12026−12032.
(34) Zhang, Y.; Zhang, X.; Situ, B.; Wu, Y.; Luo, S.; Zheng, L.; Qiu, Y. *Biosens. Bioelectron.* **2021**, *183*, 113205.
(35) Wang, R.; Zhao, X.; Chen, X.; Qiu, X.; Qing, G.; Zhang, H.; Zhang, L.; Hu, X.; He, Z.; Zhong, D.; Wang, Y.; Luo, Y. *Anal. Chem.* **2020**, *92*, 2176−2185.
(36) Kang, T.; Zhu, J.; Luo, X.; Jia, W.; Wu, P.; Cai, C. *Anal. Chem.* **2021**, *93*, 2519−2526.
(37) Liu, N.; Lu, H.; Liu, L.; Ni, W.; Yao, Q.; Zhang, G.-J.; Yang, F. *Anal. Chem.* **2021**, *93*, 5917−5923.
(38) Wu, W.; Yu, X.; Wu, J.; Wu, T.; Fan, Y.; Chen, W.; Zhao, M.; Wu, H.; Li, X.; Ding, S. *Biosens. Bioelectron.* **2021**, *175*, 112835.
(39) Lötvall, J.; Hill, A. F.; Hochberg, F.; Buzás, E. I.; Di Vizio, D.; Gardiner, C.; Gho, Y. S.; Kurochkin, I. V.; Mathivanan, S.; Quesenberry, P.; Sahoo, S.; Tahara, H.; Wauben, M. H.; Witwer, K. W.; Théry, C. *J. Extracell. Vesicles* **2014**, *3*, 26913.

https://doi.org/10.1021/acs.analchem.2c00069
Anal. Chem. 2022, 94, 5382−5391